ACS APPLIED ENGINEERING MATERIALS

pubs.acs.org/acsaenm

Article

Investigation of Nickel-Based Reforming Catalysts Under Coking Conditions in a Tailor-Made Test Setup for Performance Evaluation

Published as part of ACS Applied Engineering Materials special issue "Progresses on Materials for Solar Reforming".

Svante P. Ihrig,* Michael Wullenkord, Dimitrios Dimitrakis, Christos Agrafiotis, and Christian Sattler

Cite This: *ACS Appl. Eng. Mater.* 2025, 3, 3825−3833

Read Online

ACCESS | Metrics & More | Article Recommendations | Supporting Information

ABSTRACT: Solar reforming of biogas is a promising route for the carbon-neutral generation of syngas, with tailored fractions of hydrogen and carbon monoxide, as a versatile intermediate toward fuels and chemicals with low environmental impact, such as sustainable aviation fuels. The process features mixed steam and dry reforming, which are not yet industrially established. A catalyst test setup above lab scale was designed to facilitate catalyst performance tests and characterization under a wide range of practical conditions and to promote catalyst optimization. The catalyst test setup features a catalyst bed volume of 0.45 L and is close to industrial operation conditions, with effects such as limited heat transfer and potential pressure drop being relevant. In this setup, the feasibility of employing nickel-based catalysts for reaction conditions with increased amounts of carbon dioxide can be investigated in the temperature and absolute pressure ranges from 700 to 1000 °C and from 1 to 5 bar, respectively. With the beginning of the endothermic reforming reactions, the temperatures in the respective catalyst bed decreased by up to 100 K in comparison to the temperature of the heating source, showcasing the limited heat transfer that comes with larger setups. In addition, the setup allows the calculation of the formation rate of undesired coke at each moment during the experiment, ranging from 27.20 ± 9.78 g/min in a dry reforming experiment to 4.14 ± 4.45 g/min in a mixed reforming experiment. While methane conversion reached 73.0 ± 3.1%, carbon dioxide conversion did not exceed 28.2 ± 3.1%, highlighting the need for catalysts specifically tailored for the mixed reforming conditions and the option to test them under industrially relevant conditions as featured in the test rig introduced in this work.

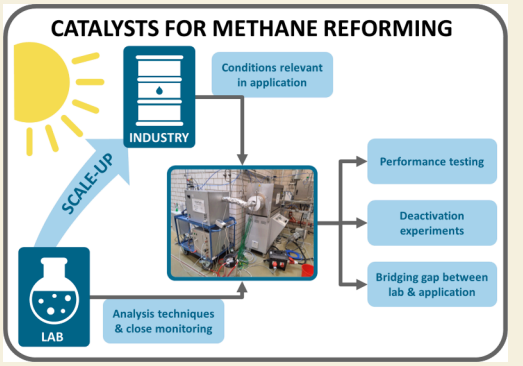

KEYWORDS: *solar mixed reforming, sustainable aviation fuels, heterogeneous catalysis, coke deposition, reforming of methane*

INTRODUCTION

In the modern world, there is a constant rise in the demand for energy. With increasing carbon emissions and the associated consequences for the climate, the need for action has been acknowledged and has led, for example, to the signing of the Paris Agreement.[1] Next to formulating goals wrt the reduction of greenhouse gas (GHG) emissions, it is necessary to provide new and improved technologies to help defossilize industries and sectors with strong emissions. One such sector is the transportation sector, producing 16% of global CO_2 emissions in 2023.[2] For private transportation, the upcoming of electric cars in combination with energy from photovoltaic or wind turbines has helped to reduce emissions.[3,4] However, for large-scale transportation, especially in the maritime and aviation sectors, this poses no promising approach. The majority of emissions in aviation stem from large aircraft and long-distance flights. Despite the continuous improvement, batteries are not energy-dense enough to support a large electrical aircraft.[5] Therefore, kerosene will still be necessary for a certain amount of time. The production of such fuels from sustainable instead of fossil sources would allow reducing emissions from the transportation sector significantly.[6] A potential production route is through the solar mixed reforming of biogas, which yields syngas (a mixture of hydrogen, H_2, and carbon monoxide, CO) that is subsequently converted by the Fischer−Tropsch synthesis into kerosene and similar products.[7,8] These sustainable aviation fuels (SAF) can be used in state-of-the-art engines and mixed with conventional kerosene in any desired ratio.[9] While steam reforming of methane, CH_4 (SRM, eq 1), from natural gas is one of the largest industrial processes, dry reforming with carbon dioxide, CO_2 (DRM, eq 2), as well as

Received: July 15, 2025
Revised: September 30, 2025
Accepted: October 6, 2025
Published: October 17, 2025

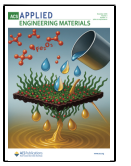

https://doi.org/10.1021/acsaenm.5c00567
ACS Appl. Eng. Mater. 2025, 3, 3825−3833

mixed steam and dry reforming (also referred to as bireforming), which allows straightforward tailoring of the syngas composition according to the requirement of the downstream process, are not yet established on a large scale.[10,11]

$$CH_4 + H_2O \leftrightarrow 3H_2 + CO \quad \Delta H^0_{298K} = +205.9\text{kJ/mol} \tag{1}$$

$$CH_4 + CO_2 \leftrightarrow 2H_2 + 2CO \quad \Delta H^0_{298K} = +247.0\text{kJ/mol} \tag{2}$$

The endothermic reactions require heat input at high process temperatures for an efficient conversion of the starting materials, usually in the range from 800 to 1000 °C. To achieve these temperatures, conventional facilities burn additional natural gas and flue gas from the process, contributing to between 3 and 20% of the natural gas consumption of the facility.[7] The use of biogas as a sustainable source of methane and carbon dioxide, as well as of renewable energies, such as concentrated solar thermal (CST) systems, to provide the heat required by the reforming reactions would therefore allow for greatly reducing the emissions of the reforming process. This heating can be performed in a direct mode, where receiver and reactor are one part,[12,13] or indirectly, where the heat is transferred from the receiver to the reactor with a heat transfer fluid (HTF), such as air or steam.[14] In combination with a heat storage unit or auxiliary heating units, indirect heating allows for a continuous 24/7 operation, therefore increasing the overall output and reducing downtime. This is especially important as syngas is only an intermediate product, although an extremely important one, that is usually fed into a subsequent process for further conversion.[10] In fact, the first preindustrial-level solar facility producing syngas with CST systems that has been recently erected and taken into operation[15] operates exactly with these concepts: indirect heating of the reforming reactor via a solar-receiver-heated gaseous HTF and high-temperature sensible heat storage of solar heat to guarantee round-the-clock continuous operation.

The processes that utilize syngas as a starting material include, for example, the Fischer−Tropsch synthesis of fuels such as gasoline, diesel, and kerosene, the synthesis of methanol, or the separation of pure hydrogen as fuel or as the starting material for the Haber−Bosch synthesis of ammonia. While the reforming reactions are favored by low pressure since the molar volume increases, most follow-up processes are more favorable under higher pressures, leading to an operation pressure for the whole facility of usually more than 25.3 bar.[8,15] To compensate for this, high-performing catalysts are necessary, which for industrial steam reforming are mostly heterogeneous catalysts based on nickel on an aluminum spinel or aluminum oxide support.[16,17] One major issue for these catalysts is the formation of coke, which occurs when the surface carbon is produced faster than it is gasified.[18,19] The production occurs mainly via the methane cracking (eq 3), while the gasification of surface carbon (C*) occurs, for example, via the Boudouard reaction (eq 4).

$$CH_4 \leftrightarrow C^* + 4H^* \tag{3}$$

$$C^* + CO_2 \leftrightarrow 2CO \tag{4}$$

These coke particles can take various shapes depending on the conditions, such as amorphous coke, graphene-like structures, or multiwalled nanotubes.[20] The growth of these structures can lead to deactivation of the catalyst by encapsulation of the nickel nanoparticles, therefore restricting access to the gas phase.[21,22] In addition, the coke can grow inside a pore of a catalyst pellet, cracking it through expansion and ultimately leading to structural failure of the catalyst bed and, therefore, reactor blockade. To circumvent these issues, in industrial conditions, a large excess of steam is utilized to suppress coke formation, which adds to the operation cost of the plant.[18] The issue of coking is even more pronounced for mixed and dry reforming due to the higher amount of carbon in the feed, which has largely contributed to its little significance in industry compared to steam reforming.[11,23] While significant scientific effort has been dedicated to resolving the issue of coke formation, many approaches involve noble metals such as palladium or rhodium, rendering them financially not feasible for large-scale applications.[24,25] Therefore, it is reasonable to exploit improvement options for nickel-based catalysts to increase their resistance toward coke formation while featuring a high conversion in a mixed or even dry reforming process. Ultimately, the usage of CST providing the process temperature for mixed reforming of biogas would allow for improving the sustainability of the process to a large extent, avoiding the employment of any fossil resources at all.

In this work, a setup above the lab scale, operating close to industrial conditions, while featuring precise temperature and pressure monitoring through various probes, is introduced and discussed. This setup allows focus on the investigation of catalysts for the process of mixed reforming at a scale bridging the lab scale and the industrial scale. While solar heating is ultimately the aim, the current reactor is heated by an electric furnace, simplifying the operation and allowing for focusing on the catalyst itself as a key component. Direct solar heating or indirect heating with an HTF might lead to inhomogeneities due to the flux distribution or turbulence in the HTF. Such temperature differences then could be falsely attributed to zones of different activities inside the catalytic bed. Hence, by reducing the complexity of the test setup and only focusing on the catalyst itself, it is possible to operate this large setup with a level of precision and monitoring as is usual in smaller lab setups.

In the following section, the construction and features of the setup are presented. Thermal tests were conducted to show the significance of temperature inhomogeneities in a potential catalyst bed and how they can be reduced with the addition of an inert particle bed. Finally, mixed reforming experiments with an exemplary commercial steam reforming catalyst are discussed, probing the potential operation conditions for such a catalyst, including the calculation of the current coke deposition rate under these conditions. All in all, this work contributes the first steps toward qualifying solar mixed reforming of biogas as an industrially relevant process by establishing a test facility that allows investigating the performance of a catalyst under close to industrial conditions, being, on the other hand, easily adaptable to indirect heating via a solar-heated HTF.

EXPERIMENTAL (METHODS AND MATERIALS)

The setup introduced in this work (Figure 1a) enables us to test reforming catalysts on a scale larger than usual lab-sized reactors, bridging the gap toward industrial scale. The central part is the custom-made reactor (Figure 1c) constructed from stainless steel (1.4841), which is positioned in a tubular electric furnace (Nabertherm, RHTH120/600/17). The reactor consists of two parts: an outer tube of 860 mm length and two compartments inside the outer tube, a cassette of 530 mm length, and a second one, which is 100 mm long (Figure 1b,d, respectively). These cassettes with a diameter of 80 mm can be filled with different materials, such as reforming catalyst pellets, chemically inert small spheres, or monolithic structures, to perform

https://doi.org/10.1021/acsaenm.5c00567
ACS Appl. Eng. Mater. 2025, 3, 3825−3833

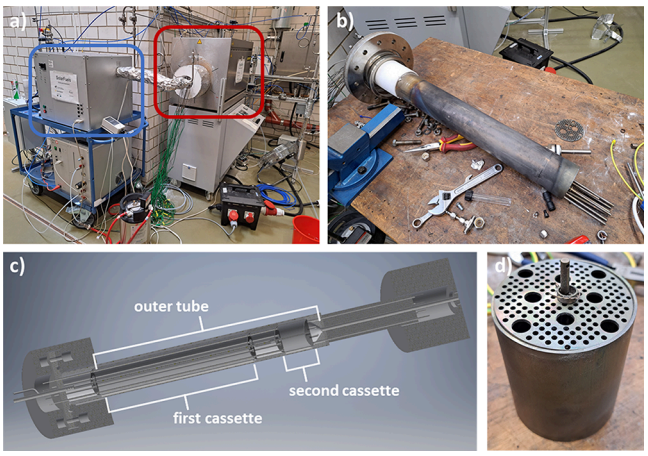

Figure 1. Overall view of the experimental setup. Highlighted components: evaporator (blue) and electric furnace with reactor (red). (b) First cassette of the reactor. (c) CAD drawing of the assembled reactor including insulation materials. (d) Second cassette of the reactor.

different types of experiments, which involve phenomena not relevant in small reactors, such as pressure drop depending on the catalyst shape or formation of hot or cold spots due to nonisothermal conditions during a reaction. The details of the performed experiments are given in more detail in later paragraphs.

A simplified scheme of the process is shown in Figure 2. The full piping and instrumentation diagram (P&ID) is given in the Supporting Information (SI). Despite the larger scale of the reactor, numerous probes are connected to the setup, which allow for close monitoring of the process. In this way, catalysts can be operated and investigated under conditions close to industrial ones, yielding insights that are not gained with small reactors where temperature distribution or mass transport are less relevant for the catalyst's performance. In its current state, operation at temperatures of up to 1000 °C (furnace set point), absolute pressures up to 5 bar, and total flow rates of 50 slpm (referring to standard conditions: 20 °C and 1.01325 bar) are possible, allowing for evaluating catalysts under a wide range of conditions.

As mentioned above, the inner part of the reactor consisted of two separate compartments. In order to closely follow the temperature changes associated with the endothermic nature of the reactions, a total of 37 type-K thermocouples (TCs) and 8 type-N TCs are placed inside the cassettes. As can be seen in Figure 3, four groups of eight TCs each are installed in the reactor at several positions along the flow axis. At each position, the temperature is measured 12.7 and 33 mm from the center axis. In this way, the radial temperature profile can be monitored, in addition to changes along the flow axis. The remaining TCs were only used for monitoring purposes and were not used for the calculation of the results.

The inlet of the reactor is connected via a heated tube with a steam evaporator (aDROP, aSTEAM DV-3). Supplied with deionized tap water (conductivity < 20 μS/cm), the evaporator provides heated steam, which is taken up by the introduced gas stream to provide the necessary reactant stream of gases. The gases available for the setup were all purchased from Linde in the stated purity, and the inflow is controlled by mass flow controllers (Bronkhorst, model AF-201AV-50K-RGD-33-V). Available gases involve nitrogen (N_2, purity 5.0), hydrogen (5.0), methane (4.5), carbon dioxide (4.5), and synthetic air (hydrocarbon-free). After mixing in the evaporator and preheating to 300 °C, the gases flow through the reactor and the catalytic bed. The reactor outlet is connected to a water cooler, reducing the temperature of the product gas to below 60 °C and removing condensed water via a gas−liquid separator. The pressure level inside the reactor is maintained via a digitally controlled back pressure regulator (Equibar, HTF series precision BPR). A portion of the gas is redistributed and analyzed with a μ-gas chromatograph (Agilent, 490 μ-GC). The remaining product gas stream is diluted with air and subsequently disposed of.

Testing of the thermal behavior: For the thermal experiments with the filled reactor, two different materials were employed. The first cassette was filled with spherical Al_2O_3 particles (Ø = 6 mm) (BASF, T-162). For the second cassette, a bed of cloverleaf-shaped SiO_2/Al_2O_3 pellets (Saint-Gobain, Denstone delta support media) was used. Pure nitrogen was used for the fluid phase. The gas was flown through the reactor with a flow rate of 5, 25, and 50 slpm at absolute pressures of 1.5, 3, and 4.5 bar and a furnace set point temperature of 725 °C. For each set of conditions, the data was recorded and averaged over 30 min once a stable state was observed.

Mixed reforming experiments: The filling of the first cassette remained the same as that for the thermal tests. The second cassette was filled with pellets of a commercial steam reforming catalyst, which is based on nickel oxide (NiO, approximately 16 wt %) on a calcium aluminate spinel support ($CaAl_2O_4$), which is recognizable in the EDX spectrum given in the SI, Figure S2a. The weight of the catalyst bed amounted to 0.5 kg in total. Activation of the catalyst was performed for 2 h with 10% H_2 in N_2 with 5 slpm total flow, and the furnace was set to 650 °C. After completion of all experiments, the catalyst was passivated at room temperature by gradually changing from the N_2 atmosphere at 2 slpm flow to pure synthetic air over the course of 2 h. For all experiments, the reactor was heated under an inert atmosphere (2 slpm N_2 flow) until the temperature set point was reached (800, 900, 950, or 1000 °C) and the temperature profile inside the reactor remained stable. Then, the nitrogen flow was closed, and methane, carbon dioxide, and steam were added to the flow in the corresponding amounts (here, an exemplary ratio $CH_4/H_2O/CO_2$ of 1.0/2.0/0.9 was applied with a total flow of 10 slpm). Once the reactor reached a steady state, data were collected and averaged over 30 min. Subsequently, the absolute pressure was adjusted to the next operation point (1, 2.5, or 4 bar). Once all pressure levels were measured at one temperature, a nitrogen flow was reestablished to purge out the remaining gases, and the furnace set point was adjusted to the next measurement point. The dry reforming experiment was conducted similarly, starting from a nitrogen atmosphere at the temperature level and changing to the reactants. Data was collected over the whole time and averaged for the corresponding GC measurement period (3 min).

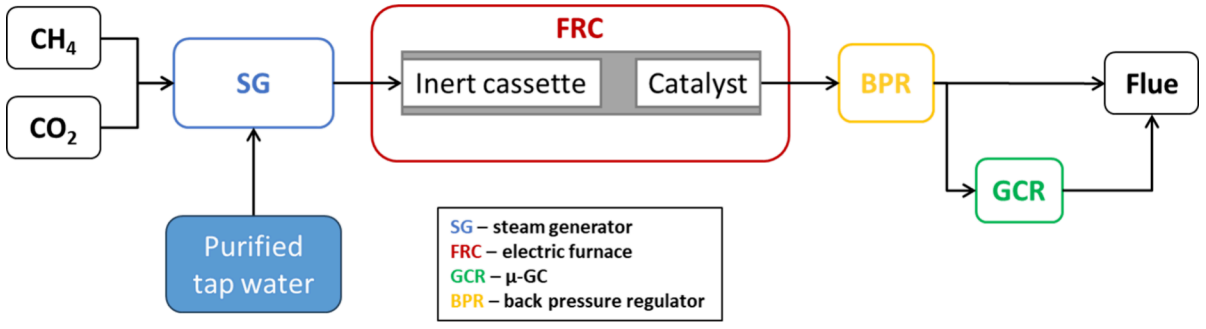

Figure 2. Simplified scheme of the test setup.

https://doi.org/10.1021/acsaenm.5c00567
ACS Appl. Eng. Mater. 2025, 3, 3825−3833

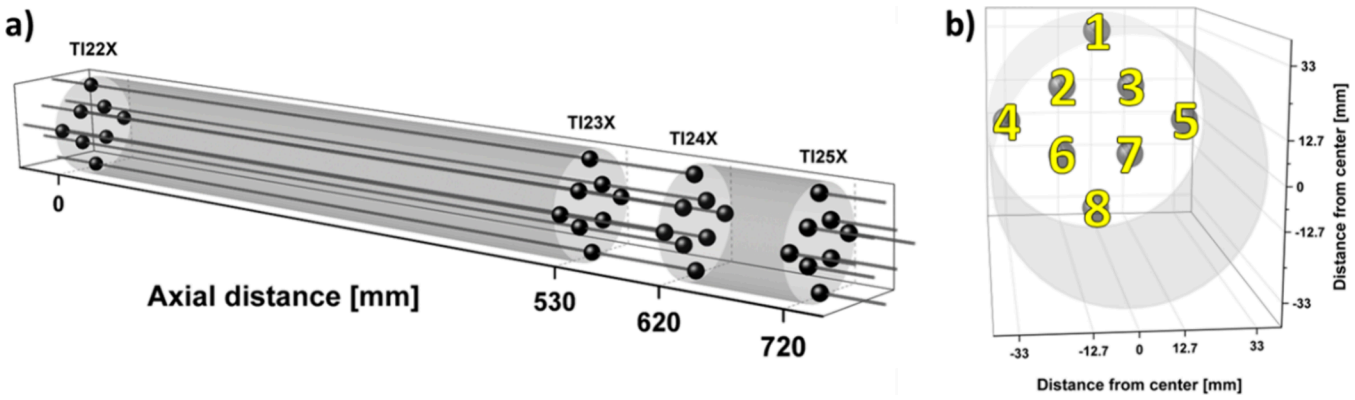

Figure 3. Schematic representation of the TC positions inside the reactor. (a) Indication of the (axial) positions of the four groups of eight TCs each, referred to as TI22X, TI23X, TI24X, and TI25X, where X points to the position of the individual TC. (b) Numbering of the eight TCs that form a group, exemplarily shown for group TI24X. As an example, the topmost TC is therefore referred to as TI241. Point of view is from the outlet of the second cassette.

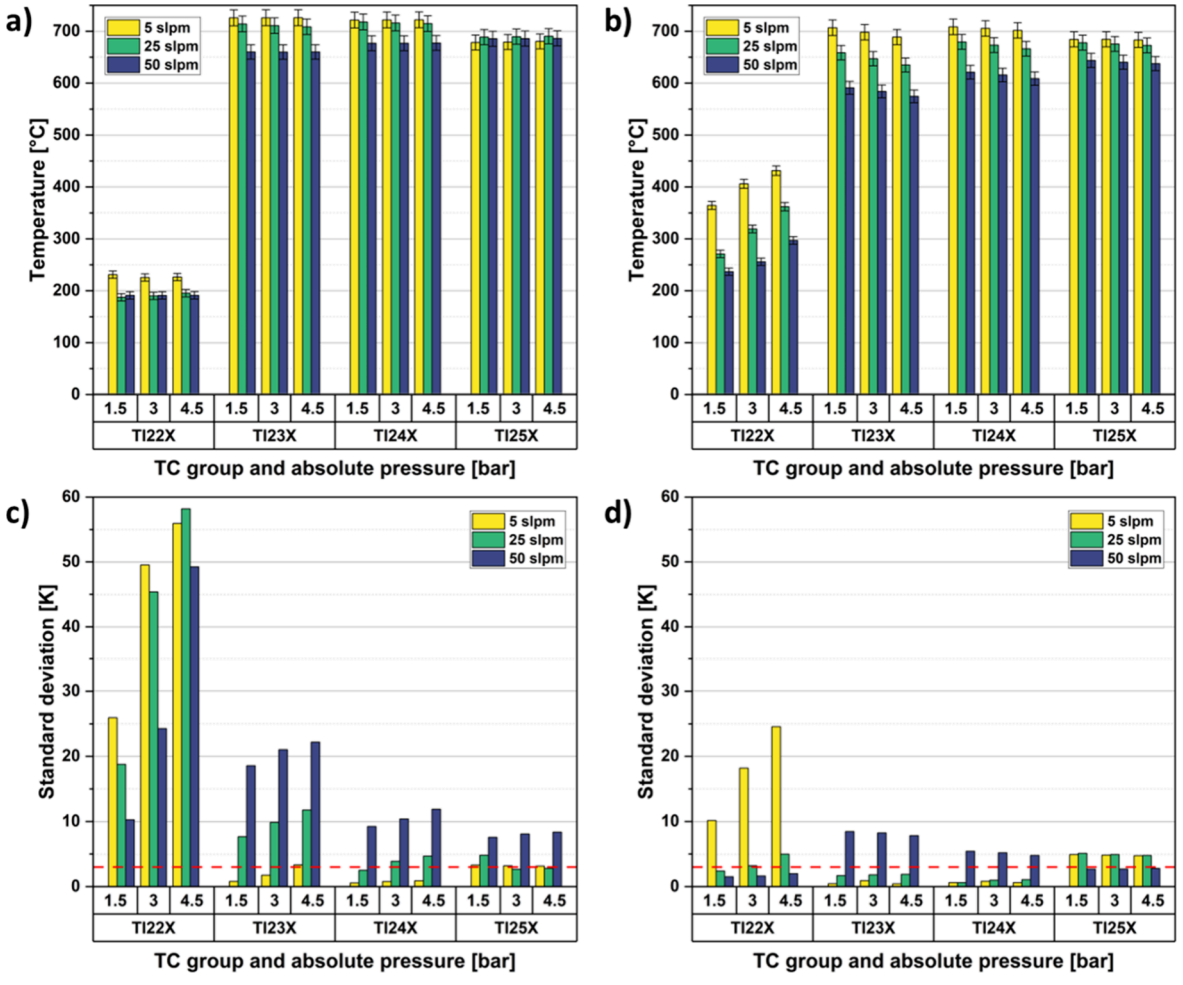

Figure 4. Axial and radial temperature distributions in the reactor cassettes at 725 °C furnace set point, nitrogen flow from 5 to 50 slpm, and absolute pressure from 1.5 to 4.5 bar. (a) Average temperatures with empty cassettes. (b) Average temperatures with both cassettes filled with inert material. (c) Standard deviations for (a) with 3σ interval marked as dashed red line. (d) Standard deviations for (b) with 3σ interval marked as dashed red line.

RESULTS AND DISCUSSION

In order to prove the validity of the design and demonstrate the significance of heat transfer in scale-up, a comparison between an empty cassette and a filled cassette was performed. At three different absolute pressure levels (1.5, 3.0, and 4.5 bar) and three flow rates (5, 25, and 50 slpm) of pure nitrogen, the average temperature and the temperature distribution at each position were measured. The results are shown in Figure 4 for a furnace set point of 725 °C, which corresponds to a lower temperature limit reasonable for reforming. Due to the endothermic nature of the reforming reactions and the limited heat transfer resulting from the size of the setup, significantly lower temperatures of the

https://doi.org/10.1021/acsaenm.5c00567
ACS Appl. Eng. Mater. 2025, 3, 3825−3833

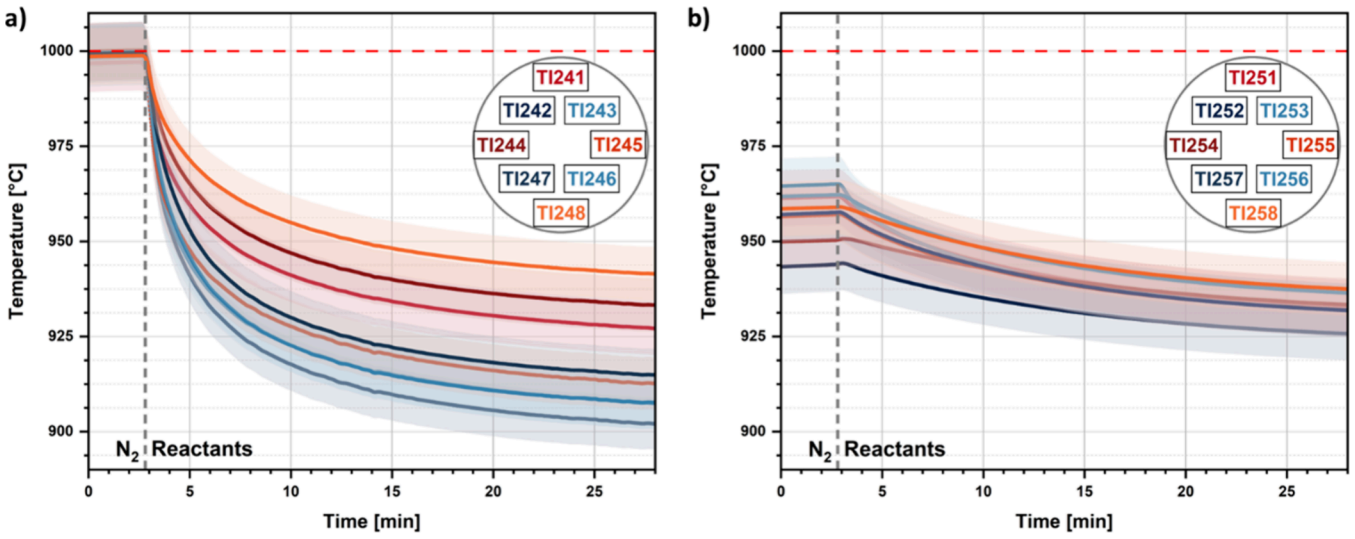

Figure 5. Temperature profile at the (a) inlet and (b) outlet of the catalyst bed (TC group TI24X for (a) and group TI25X for (b)) with the start of a mixed reforming experiment. Furnace set point 1000 °C (dashed red line), absolute pressure 1 bar, total flow 10 slpm. Change from nitrogen to reactants (molar ratio: 1.0/2.0/0.9 $CH_4/H_2O/CO_2$) was indicated by dashed gray line.

catalyst bed compared to the set point of the furnace were expected. Therefore, this relatively low temperature was chosen for the thermal experiments. With the completely empty reactor, the overall temperature lies significantly below the set point, as can be seen in Figure 4a. The lowest average temperature of the catalyst bed (TI24X and TI25X) is 609 °C, which is 116 K lower than the set point temperature of the electric furnace. In addition, it is visible that rather large discrepancies exist among the temperature readings of the eight TCs at the inlet and outlet of the catalyst cassette. Figure 4c shows the standard deviation of the temperature readings depicted in Figure 4a. The highest standard deviations are observed for the TC group TI22X, which corresponds to the entrance of the first cassette. This is well within expectations since the transition from the small-diameter tubing to the larger reactor tube leads to larger turbulences and inhomogeneities in the flow. Along the flow axis, the standard deviation decreases, indicating better homogeneity. However, most of the values remain above the 3σ confidence interval, which is indicated in the figure with the red dotted line. Both an increase in pressure and flow rate led to an increase in the standard deviation, indicating less intensive mixing and limited radial heat transfer along the stream.

To counteract heat transport limitations, the reactor cassettes were filled with a chemically inert material. The choice of the second material is attributed to its resemblance to commercial catalyst pellets, which are often uniquely shaped for reduced pressure loss and improved mass transfer. Figure 4b shows that most temperature levels increased compared to the empty reactor and were closer to the set point temperature of the furnace, apart from the TC group TI22X, which lies at the inlet of the first cassette. For the TC group TI25X with 5 slpm flow, a small decrease in the reached temperature was observed. However, under most conditions, the average temperature of the second cassette, representing the designated catalyst bed domain, was raised in comparison to the empty reactor, which is visible by 677 °C (instead of 609 °C), being the lowest average temperature among the two TC groups TI24X and TI25X. This demonstrates that the inert material helps to improve the heat transfer from the furnace to the gas stream. Additionally, from Figure 4d it becomes apparent that the temperature distribution in the radial direction is much more homogeneous compared to the empty reactor. The standard deviation is much smaller in nearly all cases and mostly within the 3σ interval. Only the TCs at the entrance of the reactor show at a low flow rate of 5 slpm a comparably high standard deviation. Interestingly, for the end of the second cassette (TI25X), a slight increase in the standard deviation is observed for 5 and 25 slpm flow, possibly hinting toward channeling effects at the reactor outlet. Nevertheless, it can be concluded beyond any doubt that the inert material in the cassettes increases the temperature of the catalyst bed and strongly reduces the thermal inhomogeneities in most positions inside the reactor. However, variations of the temperature in the radial direction remain to a certain extent and need to be considered for detailed evaluation of catalyst performance tests.

For the reforming experiments, the material in the second cassette was replaced with the nickel-based commercial catalyst mentioned above, which is originally designed for steam reforming. We conducted mixed reforming experiments under varying conditions, on the one hand, to investigate the applicability of such catalysts for the mixed reforming of biogas and, on the other hand, to demonstrate the capability of the setup. As can be extracted from Figure 5, the change from the inert nitrogen flow to the reactants of the reforming reactions leads to a strong decrease in the temperature of the catalyst bed compared to the set point of the electric furnace. While the temperature of the catalyst bed at the front (Figure 5a) is initially the same as the set point, it drops by nearly 100 K when reactants are introduced. This is attributed to the change in the heat capacity of the fluid and also the endothermic nature of the reactions (eqs 1 and 2). In the outlet of the cassette (Figure 5b), the initial temperature is lower than the set point, but the temperature decrease is also much lower compared to the one observed at the inlet of the bed, attributed to the lower reaction rates. Additionally, the radial temperature profile changes in the front from a narrow distribution to a fairly wide one, with the largest difference in temperature amounting to 40 K. As one would expect, the four inner TCs (TI242, TI243, TI246, and TI247) show larger temperature decreases compared to the outer TCs, with one exception. This is a result of the heating of the reactor tube from the outside and demonstrates how

https://doi.org/10.1021/acsaenm.5c00567
ACS Appl. Eng. Mater. 2025, 3, 3825−3833

Table 1. Operation Conditions and Corresponding Conversion of CH_4 and CO_2, STYs, Syngas Ratio, and Calculated Carbon Deposition Rate[a]

furnace set point [°C]	absolute pressure set point [bar]	average temperature of catalyst bed [°C]	conversion (CH_4)	conversion (CO_2)	STY (H_2) [mmol/(kg*h)]	STY (CO) [mmol/(kg*h)]	syngas molar ratio (H_2/CO)	coke deposition rate [g/h]
800	1.0	707.4 ± 5.3	0.599 ± 0.031	0.035 ± 0.038	6.406 ± 0.396	2.720 ± 0.118	2.355 ± 0.178	6.00 ± 4.44
800	2.5	710.3 ± 5.3	0.595 ± 0.032	0.061 ± 0.043	5.997 ± 0.382	2.523 ± 0.113	2.377 ± 0.185	10.64 ± 4.39
800	4.0	712.6 ± 5.3	0.586 ± 0.032	0.077 ± 0.043	5.720 ± 0.373	2.448 ± 0.112	2.337 ± 0.186	12.22 ± 4.38
900	1.0	810.9 ± 6.1	0.638 ± 0.033	0.110 ± 0.039	6.676 ± 0.404	3.366 ± 0.142	1.983 ± 0.146	4.14 ± 4.45
900	2.5	807.6 ± 6.0	0.664 ± 0.032	0.136 ± 0.037	6.797 ± 0.407	3.461 ± 0.146	1.964 ± 0.144	6.46 ± 4.42
900	4.0	805.8 ± 6.0	0.688 ± 0.032	0.162 ± 0.036	6.947 ± 0.410	3.567 ± 0.149	1.948 ± 0.141	8.46 ± 4.39
950	1.0	865.8 ± 6.5	0.629 ± 0.032	0.149 ± 0.037	6.322 ± 0.394	3.406 ± 0.146	1.856 ± 0.140	5.56 ± 4.41
950	2.5	862.8 ± 6.5	0.663 ± 0.032	0.185 ± 0.036	6.496 ± 0.397	3.551 ± 0.152	1.830 ± 0.136	8.42 ± 4.38
950	4.0	859.4 ± 6.4	0.696 ± 0.032	0.212 ± 0.034	6.812 ± 0.406	3.806 ± 0.160	1.789 ± 0.130	8.80 ± 4.40
1000	1.0	924.5 ± 6.9	0.636 ± 0.032	0.185 ± 0.036	6.367 ± 0.396	3.674 ± 0.157	1.733 ± 0.131	4.47 ± 4.44
1000	2.5	923.8 ± 6.9	0.688 ± 0.031	0.244 ± 0.033	6.517 ± 0.397	3.864 ± 0.166	1.687 ± 0.128	9.53 ± 4.40
1000	4.0	923.0 ± 6.9	0.730 ± 0.031	0.282 ± 0.031	6.852 ± 0.406	4.132 ± 0.174	1.658 ± 0.125	11.21 ± 4.42

[a]Total flow = 10 slpm; reactant ratio $CH_4/H_2O/CO_2$ = 1.0/2.0/0.9. Uncertainty ranges refer to the combined standard uncertainty.

temperature inhomogeneities can appear even in rather small reactors, therefore impacting catalyst performance and potentially leading to cold or hot spots. In contrast, the radial differences in temperature are much smaller at the outlet of the cassette and stay in a range comparable to values observed prior to introduction of the reactants. The observed temperature distribution emphasizes the relevance of heat transfer and the importance of local temperature measurement.

The results of the performed reforming experiments are summarized in Table 1. The space time yields (STY, see SI), representing the amount of product formed per mass of catalyst and time, take the whole mass of the catalyst into account, since the exact amount of nickel is unknown. This decision is rationalized by the varying mass of the catalyst bed, depending on the size of shape of a pellet or the porosity of a structure. The STY corrects for that and allows, therefore, the comparison of different catalysts in future experiments. Calculated STY values are also displayed in Figure 6. It becomes apparent that STY for both hydrogen and carbon monoxide increases with the temperature, but STY of carbon monoxide shows a higher sensitivity. This can potentially be attributed to the Boudouard reaction, which favors the formation of carbon monoxide with increasing temperature. Interestingly, the pressure has a negative

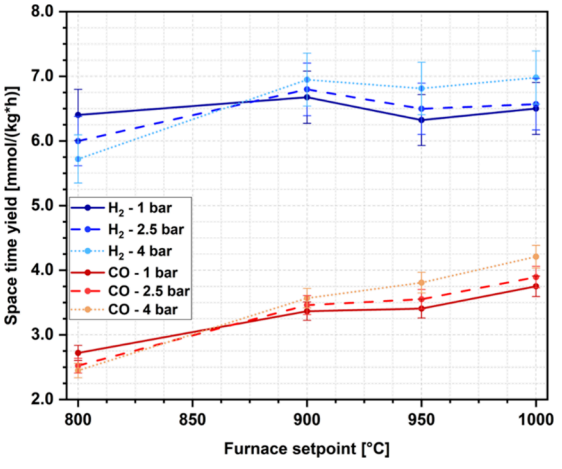

Figure 6. STYs for mixed reforming experiments for all operation conditions with a reactant composition of 1.0/2.0/0.9 (CH_4/H_2O/CO) and 10 slpm total flow.

impact on the STYs at low temperatures, and above an inversion point, the pressure influence is of a positive nature. From a thermodynamic point of view, the first observation would be expected, since the molar volume of the reaction increases and thereby should be favored by lower pressures. However, the steady state of the reactor does not reach the thermodynamic equilibrium, with significant amounts of unconverted methane and carbon dioxide. Maximum conversions (X, see the SI) of 73.0 and 28.2% were reached. Therefore, it is assumed that above this threshold temperature, the pressure increases the mass transfer and adsorption and desorption phenomena, leading to an accelerated reaction and higher STYs. Furthermore, it is seen that the syngas ratio decreases with increasing temperature, a result of the higher sensitivity toward temperature of the STY of CO.

The calculated carbon deposition rate (r_{coke}, see SI), referring to the mass balance of carbon atoms (forming part of CH_4, CO_2, and CO) at the inlet and the outlet of the reactor, is displayed in the last column of Table 1. Despite the large combined standard uncertainty, it can be concluded that coke deposition most probably took place in all except for two scenarios. In those two cases, the uncertainty is larger than the value itself, meaning that a deposition of coke on the catalyst did not necessarily occur. While the catalyst itself produces syngas under the operation conditions, the carbon deposition rate indicates a nonoptimal performance. Depending on the exact conditions, an operation duration of 100 h would lead to coke amounts comparable to the mass of the catalyst itself.

In order to demonstrate the plausibility of the calculated carbon deposition rate, a long-term coking experiment was conducted. The catalyst was subjected to dry reforming (CH_4/CO_2 ratio of 1.0/1.0) conditions at 700 °C furnace set point under atmospheric pressure for several hours to enforce coke formation in a reduced timespan. In Figure 7, STYs (a) and calculated carbon deposition rate (b) are displayed. Surprisingly, after an initial decline of the STYs, they remain nearly constant throughout more than 7 h with only a small downward tendency. This is somewhat counterintuitive in regard to the calculated coke deposition, which is significantly higher than in the previously discussed experiments.

As expected, the conditions of dry reforming led to an increased formation of coke. Two stages can be distinguished in Figure 7b. First, a sharp increase in the carbon formation rate is

https://doi.org/10.1021/acsaenm.5c00567
ACS Appl. Eng. Mater. 2025, 3, 3825−3833

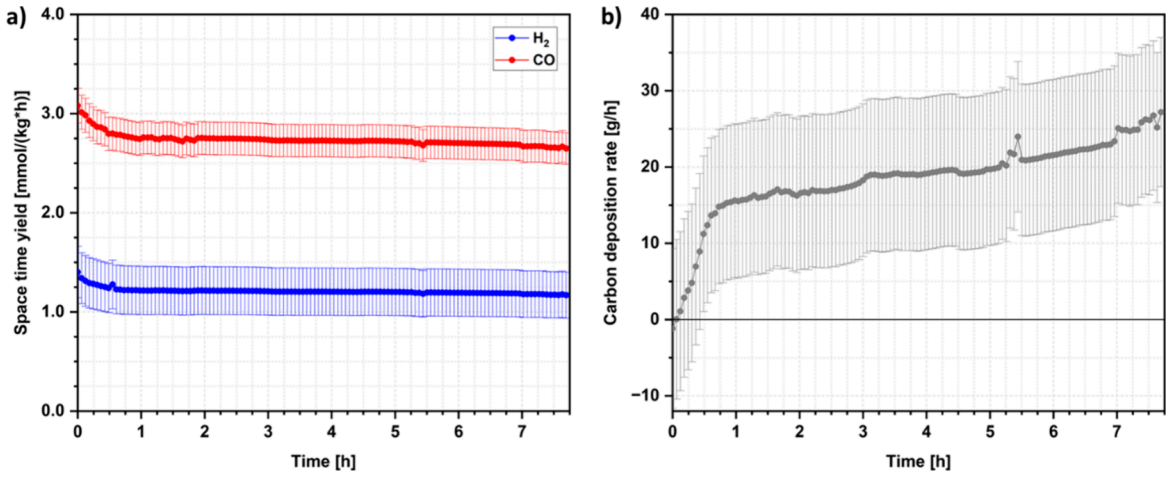

Figure 7. (a) STYs for a prolonged dry reforming experiment. (b) Calculated coke deposition rate for prolonged dry reforming experiment. Dry reforming was conducted with a CH_4/CO_2 ratio of 1 and a total flow of 10 slpm. Operation at 700 °C furnace set point and under atmospheric pressure.

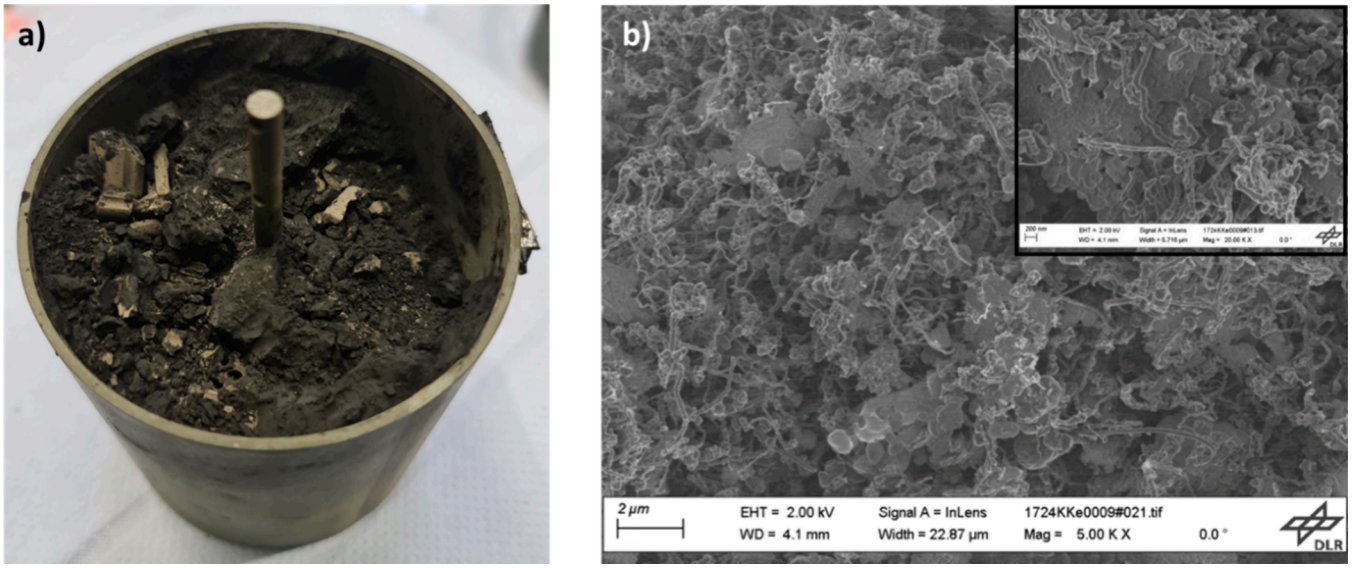

Figure 8. Catalyst bed after completion of dry reforming experiment with CH_4/CO_2 ratio of 1, total flow of 10 slpm, and a duration of 8 h. (a) Visible is the inlet of the second cassette where the gas stream enters the catalytic bed. Parts of the deposited coke and broken catalyst pellets were removed to a depth of about 1 cm. Remains of the catalyst pellets with different structural integrity are visible. (b) SEM image (2 μm scale) of a sample taken from the catalyst bed. Inset shows an area of the same sample under a higher magnification (200 nm scale).

observed, which is attributed to the nucleation phase.[26] Second, a high but more stable deposition rate can be seen with only a small increase over the reaction time, reaching a maximum value of 27.20 ± 9.78 g/min after more than 7 h of operation. In combination with the near-constant STYs, this indicates that the deactivation of the catalyst takes longer than the timespan of the experiment covered. However, removal of the cassette holding the catalytic bed showed a massive formation of coke, resulting in one large block (Figure 8a). SEM investigations show the many carbon nanotubes that have formed, visible as string-like structures in Figure 8b. The catalyst pellets were mostly crushed; only in the middle part of the cassette did some pellets remain complete. It is interesting that despite the apparently solid plug formed, not only was there no measurable drop in pressure observed, but the STYs were also unchanged, demonstrating the complexity of the process of deactivation. The changes in STY alone would not have indicated such a deposition, highlighting that monitoring changes in the coke deposition rate helps to predict the deactivation of a catalyst.

Altogether, these experiments demonstrate the capability of the setup, combining close monitoring of a lab experiment with the conditions and relevant phenomena of a large-scale application in industry. The established method to directly follow the deposition of coke via mass balancing of carbon in a bed of catalyst pellets, similar to industrial reactors, will allow the gain of valuable insights into the operation of such catalysts and potential improvements for catalyst design.

CONCLUSIONS

A setup for the testing of reforming catalysts to produce syngas, with a catalyst bed volume of 0.45 L, on a scale going above typical lab-scale reactors was introduced. This test rig enables the assessment of catalyst performance under operation conditions that lie closer to industrial ones, with important phenomena such as heat and mass transfer limitations as well as pressure drop potentially taking place that are not observed on the smaller scale. With electrical furnace set point temperatures

https://doi.org/10.1021/acsaenm.5c00567
ACS Appl. Eng. Mater. 2025, 3, 3825−3833

up to 1000 °C and absolute pressures up to currently 5 bar, a wide range of reaction conditions can be investigated. It was demonstrated that an upstream bed of chemically inert material clearly enhances heating of the gas stream prior to reaching the catalyst bed, allowing higher temperatures and generally a significant reduction of temperature differences in the catalyst domain. A commercial, nickel-based catalyst designed for steam reforming was exemplarily used to perform mixed (steam and dry) and dry reforming experiments. It was shown that even in a comparatively small reactor, the temperature of the catalyst bed is in the steady state significantly lower than the temperature of the employed heating source, showcasing the limiting heat transfer of upscaled reactors. The STYs of H_2 and CO were calculated, both increasing with temperature. The conversion of CH_4 and CO_2 shows the same trend, but the conversion of CO_2 remained at overall low levels with no more than 28.2 ± 3.1% compared to the conversion of up to 73.0 ± 3.1% for CH_4. The pressure shows a changing influence depending on the temperature. During the production of syngas using a catalyst, the deposition rate of coke was estimated continuously as an important indicator for long-term operation. A dry reforming experiment was conducted over several hours to force coke deposition and verify the plausibility of the calculated carbon deposition rates. While the STYs for H_2 and CO showed only a little decline and remained stable throughout the experiment, different phases were observed regarding the carbon deposition rate. An initial strong increase, associated with the nucleating phase, and a second slower increasing phase were identified. An overall high coke deposition rate was confirmed by visual inspection of the cassette and SEM investigation following the experiment, showing large amounts of coke that even led to the destruction of the catalyst bed. This observation demonstrates how deactivation processes take place prior to a notable performance decline, highlighting the importance of monitoring these rates in larger setups and tailored catalyst designs.

A valuable facility has been introduced, which helps to bridge the gap between the lab and industrial scale. The operation at higher pressure and a catalyst bed with pellets rather than a powder is close to industrial conditions, while the comprehensive temperature measurement and analysis of a lab reactor is given. This allows deeper insight into the performance of catalysts under conditions relevant for large-scale applications and investigating practical catalyst optimization options. While the exemplary assessment of a commercial catalyst showcased the capabilities of the setup, future improvements, including other reforming methods, such as trireforming, also employing oxygen,[27] or theoretical assistance with simulation methods, will help to further widen its possibilities and provide valuable support for catalyst optimization and the transfer of academic solutions toward industrial applications.

■ ASSOCIATED CONTENT

Supporting Information

The Supporting Information is available free of charge at https://pubs.acs.org/doi/10.1021/acsaenm.5c00567.

Calculation of values, P&ID of the setup, and EDX spectra of unused catalyst and after experiments (PDF)

■ AUTHOR INFORMATION

Corresponding Author

Svante P. Ihrig − *Institute of Future Fuels, German Aerospace Center (DLR), Juelich 52428, Germany;* orcid.org/0000-0001-7848-9246; Email: svante.ihrig@dlr.de

Authors

Michael Wullenkord − *Institute of Future Fuels, German Aerospace Center (DLR), Juelich 52428, Germany*

Dimitrios Dimitrakis − *Institute of Future Fuels, German Aerospace Center (DLR), Juelich 52428, Germany;* orcid.org/0000-0002-1666-5942

Christos Agrafiotis − *Institute of Future Fuels, German Aerospace Center (DLR), Cologne 51147, Germany*

Christian Sattler − *Institute of Future Fuels, German Aerospace Center (DLR), Cologne 51147, Germany*

Complete contact information is available at: https://pubs.acs.org/10.1021/acsaenm.5c00567

Author Contributions

The manuscript was written through contributions of all authors. All authors have given approval to the final version of the manuscript.

Notes

The authors declare no competing financial interest.

■ ACKNOWLEDGMENTS

The contents of this article are based on the project SolarFuels, which is funded by the Federal Ministry for Economic Affairs and Climate Action of Germany (grant number 03EE5085B). We would like to thank Kai-Peter Eßer for his vast support in assembly and operation of the setup, Anna-Maria Franzen, Jonas Rehrmann, Marie Heisterkamp, and Marcel Kloft for the valuable support during the experiments, and Liudmila Chernova for the SEM images and measurement of the EDX spectra.

■ ABBREVIATIONS

CST,concentrated solar thermal; DRM,dry reforming of methane; EDX,energy-dispersive X-ray spectroscopy; GC,gas chromatograph; GHG,greenhouse gases; HTF,heat transfer fluid; P&ID,piping and instrumentation diagram; SAF,sustainable aviation fuels; SEM,scanning electron microscopy; SI,Supporting Information; SRM,steam reforming of methane; STY,space time yield; TC,thermocouple

■ REFERENCES

(1) *United Nations*; Paris Agreement, **2015**.

(2) Liu, F.; Shafique, M.; Luo, X. Next leap in the sustainable transport revolution: Identifying gaps and proposing solutions for hydrogen mobility. *Communications in Transportation Research* **2025**, *5*, No. 100180.

(3) Tsakalidis, A.; Thiel, C.; Jäger-Waldau, A. Can solar electric vehicles disrupt mobility? A critical literature review. *Renewable ans Sustainable Energy Reviews* **2025**, *211*, No. 115289.

(4) Ahmed, I.; Basit, A.; Ahmad, M.; AlMuhaini, M.; Khalid, M. Electric Mobility Challenges and Approaches for Sustainable Green Power Synergy in Smart Cities. *Arabian Journal for Science and Engineering* **2025**, *50*, 5323−5351.

(5) Viswanathan, V.; Epstein, A. H.; Chiang, Y.-M.; Takeuchi, E.; Bradley, M.; Langford, J.; Winter, M. The challenges and Opportunities of battery-powered flight. *Nature* **2022**, *601* (7894), 519−525.

(6) Song, G.; An, H.; Hou, Y.; Tong, H.; Liu, J.; Tang, X.; Yi, H. Review of the historical trends and decarbonization pathways of the civil aviation sector. *Renewable and Sustainable Energy Reviews* **2025**, *222*, No. 115927.
(7) Agrafiotis, C.; Wullenkord, M.; Roeb, M.; Sattler, C. Chapter Three - Solar thermal methane reforming. *Adv. Chem. Eng.* **2021**, *1*, 91−130.
(8) Agrafiotis, C.; von Storch, H.; Roeb, M.; Sattler, C. Solar thermal reforming of methane feedstocks for hydrogen and syngas production - A review. *Renewable and Sustainable Energy Reviews* **2014**, *29*, 656−682.
(9) Raji, A. M.; Manescau, B.; Chetehouna, K.; Lamoot, L.; Ogabi, R. Overview of combustion and emission characteristics of sustainable aviation fuels and standard JET A-1 fuel. *Fuel* **2025**, *402*, No. 136011.
(10) Rostrup-Nielsen, J. R.; Sehested, J. Hydrogen and Synthesis Gas by Steam- and CO_2 Reforming. *Adv. Catal.* **2002**, *47*, 65−139.
(11) Wang, Z.; Mei, Z.; Wang, L.; Wu, Q.; Xia, C.; Li, S.; Wang, T.; Liu, C. Insight into the activity of Ni-based thermal catalysts for dry reforming of methane. *Journal of Materials Chemistry A* **2024**, *12*, 24802.
(12) Buck, R.; Muir, J. F.; Hogan, R. E. Carbon dioxide reforming of methane in a solar volumetric receiver/reactor: the CAESAR project. *Solar Energy Materials* **1991**, *24* (1−4), 449−463.
(13) Wörner, A.; Tamme, R. CO2 reforming of methane in a solar driven volumetric receiver−reactor. *Catal. Today* **1998**, *46* (2−3), 165−174.
(14) Hernández, B.; Ferber, N. L.; Abdullah, M.; Mayyas, A.; Calvet, N.; Chiesa, M. Central receiver-based CSP plants Part 2: Components categorization amd future prospects. *Sol. Energy* **2025**, *299*, No. 113740.
(15) Synhelion, *Synhelion inaugurates DAWN − the world's first industrial plant for the production of solar fuels*, Jülich, 2024.
(16) Jang, W.-J.; Jeong, D.-W.; Shim, J.-O.; Kim, H.-M.; Roh, H.-S.; Son, I. H.; Lee, S. J. Combined steam and carbon dioxide reforming of methane and side reactions: Thermodynamic equilibrium analysis and experimental application. *Applied Energy* **2016**, *173*, 80−91.
(17) Arman, A.; Hagos, F. Y.; Abdullah, A. A.; Mamat, R.; Aziz, A. R. A.; Cheng, C. K. Syngas production through steam and CO2 reforming of methane over Ni-based catalyst - A Review. IOP Conf. Series. *Materials Science and Engineering* **2020**, *736*, No. 042032.
(18) Rostrup-Nielsen, J. R. Catalytic Steam Reforming. *Catalysis*; Springer, 1984; pp 1−117.
(19) Geng, Z.; Gao, J.; Dong, H.; Wang, S.; Zhang, M. The role of water in bi-reforming of methane: a micro-kinetic study. *Reaction Kinetics, Mechanisms and Catalysis* **2022**, *135*, 705−721.
(20) Snoeck, J.-W.; Froment, G. F.; Fowles, M. Kinetic Study of the Carbon Filament Formation by Methane Cracking on a Nickel Catalyst. *J. Catal.* **1997**, *169*, 250−262.
(21) Ochoa, A.; Bilbao, J.; Gayubo, A. G.; Castano, P. Coke formation and deactivation during catalytic reforming of biomass and waste pyrolisis products: A review. *Renewable and Sustainable Energy Reviews* **2020**, *119*, No. 109600.
(22) Zhou, L.; Li, L.; Wei, N.; Li, J.; Basset, J.-M. Effect of NiAl2O4 Formation on Ni/Al2O3 Stability during Dry Reforming of Methane. *ChemCatChem.* **2015**, *7*, 2508−2516.
(23) Mortensen, P. M.; Dybkjær, I. Industrial scale experience on steam reforming of CO2-rich gas. *Applied Catalysis A: General* **2015**, *495*, 141−151.
(24) Niu, J.; Guo, F.; Ran, J.; Qi, W.; Yang, Z. Methane dry (CO2) reforming to syngas (H2/CO) in catalytic process: From experimental study and DFT calculations. *Int. J. Hydrogen Energy* **2020**, *45*, 30267−30287.
(25) Jones, G.; Jakobsen, J. G.; Shim, S. S.; Kleis, J.; Andersson, M. P.; Rossmeisl, J.; Abild-Pedersen, F.; Bligaard, T.; Helveg, S.; Hinnemann, B.; Rostrup-Nielsen, J. R.; Chorkendorff, I.; Sehested, J.; Nørskov, J. K. First principles calculations and experimental insight into methane steam reforming over transition metal catalysts". *J. Catal.* **2008**, *259*, 147−160.
(26) Snoeck, J.-W.; Froment, G. F.; Fowles, M. Filamentous Carbon Formation and Gasification: Thermodynamics, Driving Force, Nucleation and Steady-State Growth. *J. Catal.* **1997**, 240−249.
(27) Soleimani, S.; Lehner, M. Tri-Reforming of Methane: Thermodynamics, Operation Conditions, Reactor Technology and Efficiency Evaluation - A Review. *Energies* **2022**, *15*, 7159.

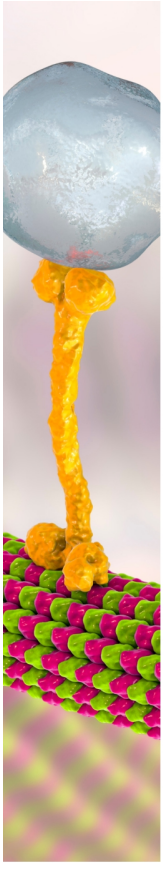

https://doi.org/10.1021/acsaenm.5c00567
ACS Appl. Eng. Mater. 2025, 3, 3825−3833